scientific reports

Check for updates

OPEN

Structure and selected properties of Al–Cr–Fe alloys with the presence of structurally complex alloy phases

K. Młynarek-Żak[1]✉, W. Pakieła[1], D. Łukowiec[1], A. Bajorek[2], P. Gębara[3], A. Szakál[4], I. Dhiman[4] & R. Babilas[1]✉

The aim of the study was to supplement the data on the $Al_{65}Cr_{20}Fe_{15}$ alloy with binary phase structure and the $Al_{71}Cr_{24}Fe_5$ alloy with multiphase structure prepared with two different cooling rates from the liquid state. The presence of the structurally complex $Al_{65}Cr_{27}Fe_8$ phase was confirmed by neutron diffraction, scanning electron microscopy with the analysis of chemical composition and transmission electron microscopy. Additionally, the Al_8Cr_5 phase with γ-brass structure was identified for $Al_{71}Cr_{24}Fe_5$ alloy in both cooling rates from the liquid state. Due to the interesting features of structurally complex alloys, the wear resistance, magnetic properties, and corrosion products after performing electrochemical tests were examined. Based on pin-on-disc measurements, a lower friction coefficient was observed for the $Al_{65}Cr_{20}Fe_{15}$ alloy ($\mu \approx 0.55$) compared to the $Al_{71}Cr_{24}Fe_5$ multiphase alloy ($\mu \approx 0.6$). The average hardness of the binary phase $Al_{65}Cr_{20}Fe_5$ alloy ($HV_{0.1} = 917 \pm 30$) was higher compared to the multiphase $Al_{71}Cr_{24}Fe_5$ alloy ($HV_{0.1} = 728 \pm 34$) and the single phase Al–Cr–Fe alloys described in the literature. Moreover, the beneficial effect of rapid solidification on hardness was demonstrated. The alloys $Al_{65}Cr_{20}Fe_{15}$ and $Al_{71}Cr_{24}Fe_5$ showed paramagnetic behavior, however rapidly solidified $Al_{71}Cr_{24}Fe_5$ alloy indicated an increase of magnetic properties. The studied alloys were characterized by the presence of passive layers after electrochemical tests. A higher amount of oxides on the surface of the $Al_{71}Cr_{24}Fe_5$ alloy was recorded due to the positive effect of chromium on the stabilization of the passive layer.

Complex metallic alloys (CMAs) are intermetallic crystalline compounds. CMAs are composed of structurally complex alloy phases (SCAPs)[1]. They are characterized by large unit cells that can be made up of thousands of atoms. Crystals that contain several dozen atoms in their cell[2], quasicrystals, and their approximants[3] are considered SCAP-type structures. Complex metallic alloys indicate interesting physicochemical properties, such as high hardness, low friction coefficient, and good corrosion resistance[4,5]. Moreover, SCAPs free from structure defects can be characterized by a high degree of magnetic order[6]. The set of unique characteristics of alloys with the structurally complex structure results from differences in the transport of electrons and phonons due to the different atomic structures of classical crystal lattices[2,7]. The main limitations for the development of this group of materials is the manufacturing of structurally complex single-phase alloys and the computational and theoretical resources for their description[6]. Based on physicochemical properties, complex metallic alloys have potential applications as thermoelectric, catalytic, and structural materials (among others, in high-load satellite parts)[3,5,6]. CMAs could be applied in composites or as coating materials due to the reduced friction coefficient[4,5,8].

The Al–Cr–Fe, Al–Cu–Fe and Al–Cu–Fe–Cr alloys were classified as CMAs due to the presence of a structurally complex alloy phases[4]. The occurrence of γ-brass phases was often observed during the preparation of quasicrystals and their approximants in Al–Cr[9,10], Al–Cr–Fe[2,4,8,11–14], Al–Cu[15,16], and Al–Cu–Cr[17,18] chemical compositions[12]. Dong[9] stated that the γ-brass phases are approximations to quasicrystals. Similarly, Veys et al.[19] indicated that the phase of $Al_{65}Cr_{27}Fe_8$ is a CMA compound with γ-brass structure that can be considered

[1]Department of Engineering Materials and Biomaterials, Silesian University of Technology, Konarskiego 18a, 44-100 Gliwice, Poland. [2]A. Chełkowski Institute of Physics, University of Silesia in Katowice, 75 Pułku Piechoty 1, 41-500 Chorzów, Poland. [3]Department of Physics, Częstochowa University of Technology, Armii Krajowej 19, 42-200 Częstochowa, Poland. [4]Budapest Neutron Centre, Konkoly-Thege Miklos st. 29-33, Budapest 1121, Hungary. ✉email: katarzyna.mlynarek-zak@polsl.pl; rafal.babilas@polsl.pl

as an approximant of quasicrystalline icosahedral and decagonal phases. In other publications[4,11], the alloys $Al_{64.2}Cr_{27.2}Fe_{8.1}$ and $Al_{66.9}Cu_{11.6}Fe_{11.6}Cr_{10.6}$ of structurally complex alloys were produced by hot sintering powders in the form of rolls with a diameter of 20 mm and then subjected to heat treatment. Based on the X-ray diffraction analysis, the Al_8Cr_5 phase was identified for the $Al_{64.2}Cr_{27.2}Fe_{8.1}$ alloy and $Al_{6.5}Cr_{0.5}Cu_2Fe$ phase for the $Al_{66.9}Cu_{11.6}Fe_{11.6}Cr_{10.6}$ alloy. The authors[11] concluded that the Al_8Cr_5 phase (γ-brass) is isostructural with the $Al_{65}Cr_{27}Fe_8$ phase.

The purpose of the work was to provide detailed structural studies of the $Al_{65}Cr_{20}Fe_{15}$ and $Al_{71}Cr_{24}Fe_5$ alloys produced with two different cooling rates from the liquid state. In addition to the earlier work[20], these alloys have not been described in terms of structure so far. Moreover, there is still a few experimental data that confirm the interesting properties of Al–Cr–Fe alloys with the CMAs, especially with binary and multiphase structure[4,5]. The results of the selected properties such as wear resistance, hardness, magnetic behavior, and chemical composition of the surface after corrosion were analyzed.

Materials and methods

Chemical elements of Al, Cr, and Fe with a purity of 99.99% were melted in an induction furnace with appropriate atomic fractions ($Al_{71}Cr_{24}Fe_5$ and $Al_{65}Cr_{20}Fe_{15}$ at.%) in a protective argon atmosphere in corundum crucibles (Φ = 30 mm, H = 45 mm) and then Ar-cooled. Ingots produced with a weight of 50 g were remelted and cast with an increased cooling rate from a liquid state under pressure (high-pressure die casting method with a cooling rate ~ 10^3 K/s) to a water-cooled copper mold (90 × 80 × 45 mm) in the form of plates (30 × 10 × 1 mm). X-ray diffraction, light microscopy observations, Mössbauer spectroscopy, differential scanning calorimetry, and electrochemical measurements were described for these alloys in an earlier publication[20].

Neutron diffraction studies were performed on the MTEST neutron powder diffractometer at the Budapest Neutron Center. The Cu(111) monochromator was used which selected neutrons with a wavelength of λ = 0.1446 nm. The measured 2θ range was between 10° and 140°. This setup allowed a sufficient q-range and resolution for the identification of different phases present in the samples.

Observations of an ingot structure were made using scanning electron microscopy in backscattered electron (BSE) mode (Supra 35, Carl Zeiss) with EDX analysis to identify maps with the chemical composition of phases.

High resolution transmission electron microscopy (HRTEM) was used to determine electron diffraction from the selected area (SAED), structure, and morphology using S/TEM TITAN 80–300. Samples for HRTEM observations were powdered.

Coercive force (H_c) and saturation magnetization (M_s) were determined from changes of magnetization as a function of the magnetic fields up to 10 kOe. Magnetic properties were recorded using a LakeShore 7307 vibrating sample magnetometer.

Tribological tests were performed using the pin-on-disc method using CSM Instruments. The experiments were carried out on cylindrical ingots with a radius of 26 mm and a height of 3 mm. The radius of the wear track was 8 mm. A ball made of 100C6 steel with a diameter of 6 mm was used as a counter-sample. The linear speed was 0.01 m/s and a load of 10 N was applied. Observations of the wear tracks, together with measurements of their width after tribological tests, were carried out by scanning electron microscope (Supra 35, Carl Zeiss). Hardness tests were performed using a Future Tech FM-700 Vickers hardness testing instrument with a load of 100 g for 15 s.

The corrosion products on the surface of the $Al_{65}Cr_{20}Fe_{15}$ and $Al_{71}Cr_{24}Fe_5$ samples in the form of plates after corrosion tests in 3.5% NaCl solution at 25 °C were determined by X-ray photoelectron spectroscopy (XPS). Depth profile mode (DP-XPS) using a Physical Electronics (PHI 5700/660) spectrometer working under an ultra-high vacuum (10^{-9} Torr) in UHV cluster and a monochromatic Al Kα X-ray source (1486.6 eV) was used. Both tested samples were initially kept pre-chamber held under vacuum (10^{-8} Torr) for at least 1 h, next transferred to the measurement chamber and analyzed. The survey spectra were measured with a pass energy of 187.85 eV. Depth profile (DP-XPS) analysis was carried out using a focused 1.5 kV Ar^+ beam for 15 min, sputtering in intervals between measurements. Core-level lines collected in the DP-XPS analysis were measured with a pass energy of 23.5 eV. All obtained XPS data was analyzed using MultiPak 9.7 software, which contains an internal reference database and compared to the NIST XPS database.

Ethical approval. This article does not contain any studies with human participants or animals performed by any of the authors.

Results and discussion

Based on the phase analysis provided by the XRD method presented in[20], the $Al_{65}Cr_{20}Fe_{15}$ alloy was characterized by a binary phase structure (ingot: $Al_{65}Cr_{27}Fe_8$ (SCAP) + $Al_{12.59}Fe_{6.41}$, plate: $Al_{65}Cr_{27}Fe_8$ (SCAP) + $Al_{5.6}Fe_2$), and the $Al_{71}Cr_{24}Fe_5$ alloy, a multiphase (ingot: Cr + $Al_{65}Cr_{27}Fe_8$ (SCAP) + $Al_{8.26}Cr_{4.74}$ + Al_2Cr + Fe_2CrAl + Al_8Cr_5 + $Al_{45}Cr_7$, plate: Cr + $Al_{65}Cr_{27}Fe_8$ (SCAP) + $Al_{8.26}Cr_{4.74}$ + Al_2Cr + Fe_2CrAl + Al_8Cr_5 + $Al_{45}Cr_7$). The presence of the identified phases in the structure for the ingots was confirmed by the analysis of the neutron diffractograms in Fig. 1. The presence of the Fe_2CrAl and Cr phases was excluded for $Al_{71}Cr_{24}Fe_5$ due to the small number of matched reflections. Furthermore, observations were carried out using scanning electron microscopy in BSE mode with the EDX analysis presented in Fig. 2 for $Al_{65}Cr_{20}Fe_{15}$ and Fig. 3 for $Al_{71}Cr_{24}Fe_5$ alloys. SEM observations confirmed the presence of two phases in the structure of the $Al_{65}Cr_{20}Fe_5$ alloy. The presented EDX maps allow us to suppose that the alloy matrix was constituted by the $Al_{65}Cr_{27}Fe_8$ (SCAP) phase, while the role of reinforcing phase was played by $Al_{12.59}Fe_{6.41}$. Identification of individual phases of the $Al_{71}Cr_{24}Fe_5$ alloy was difficult due to the presence of many phases. However, iron-rich areas were identified suggesting the presence of the $Al_{65}Cr_{20}Fe_8$ (SCAP) phase. The Al–Cr phases formed a dendritic structure.

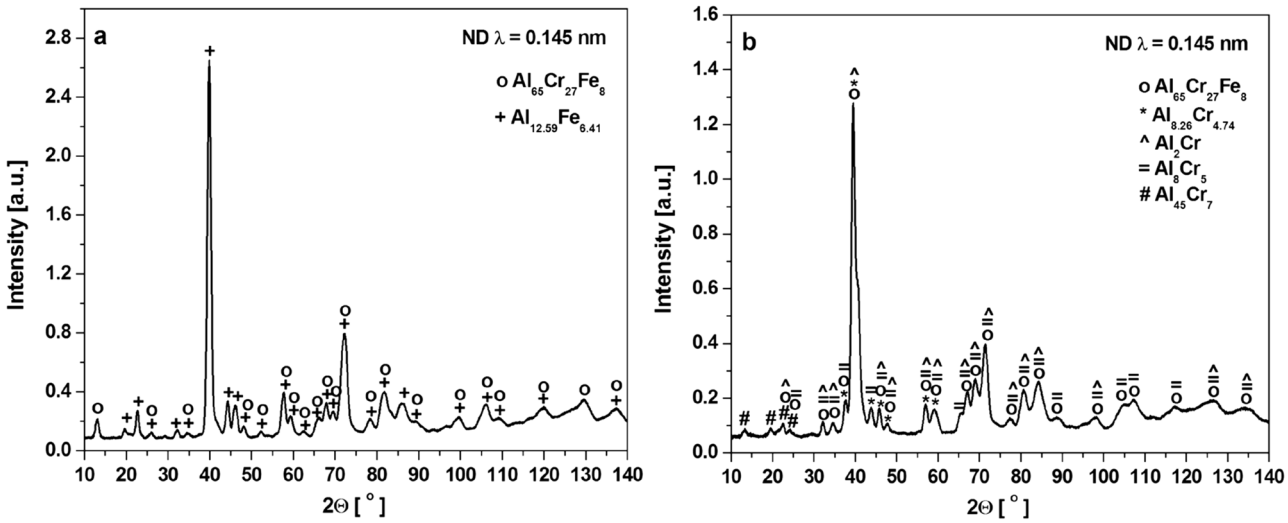

Figure 1. ND patterns of $Al_{65}Cr_{20}Fe_{15}$ (**a**) and $Al_{71}Cr_{24}Fe_5$ (**b**) alloys in a form of ingot.

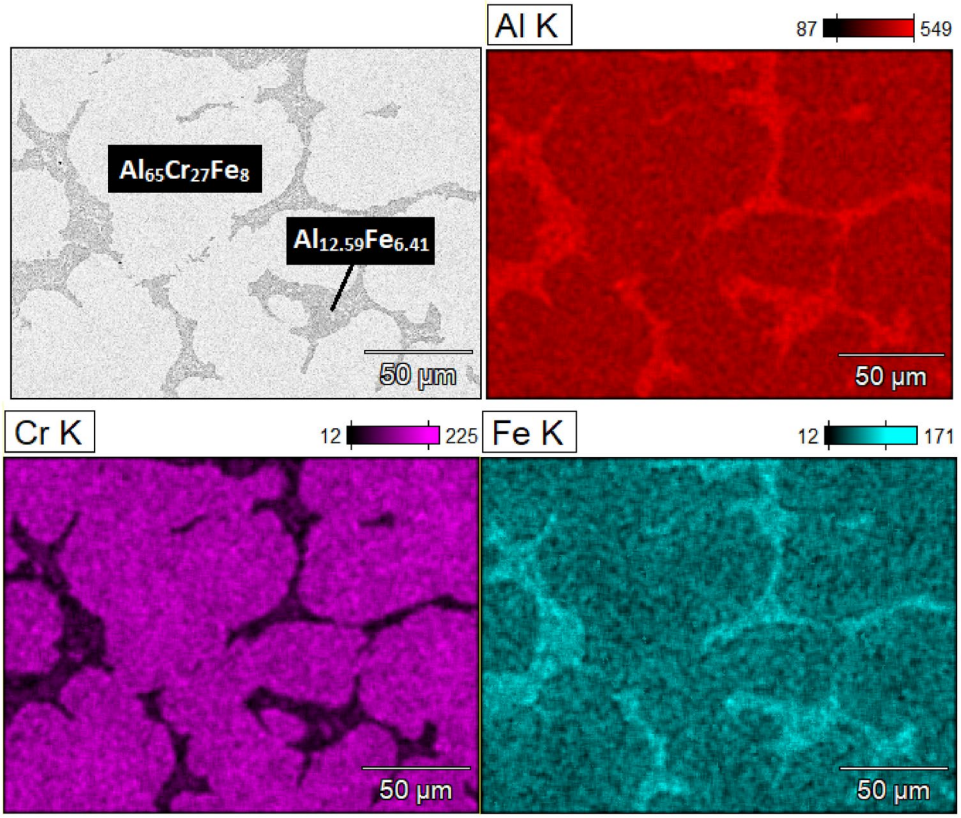

Figure 2. EDX maps of $Al_{65}Cr_{20}Fe_{15}$ alloy in a form of ingot.

In addition, studies with the use of transmission electron microscopy, presented in Figs. 4 and 5, were carried out. The presence of two phases in the structure of the $Al_{65}Cr_{20}Fe_{15}$ alloy and multiple phases in $Al_{71}Cr_{24}Fe_5$ was confirmed by selected area electron diffraction (SAED) patterns from the areas of Figs. 4a and 5a. TEM investigations were performed for samples in a form of plate. SAED analysis confirmed the ND results. The Inverse Fourier Transform (IFT) images also show areas with an ordered structure of atoms, characteristic of crystalline structures. The interplanar spacings in the marked crystalline areas were $d = 0.458$ nm (Fig. 4b) and $d = 0.368$ nm (Fig. 5b). The revealed values of the d spacings were found to closely with the interplanar spacings of the $Al_{65}Cr_{27}Fe_8$ phase.

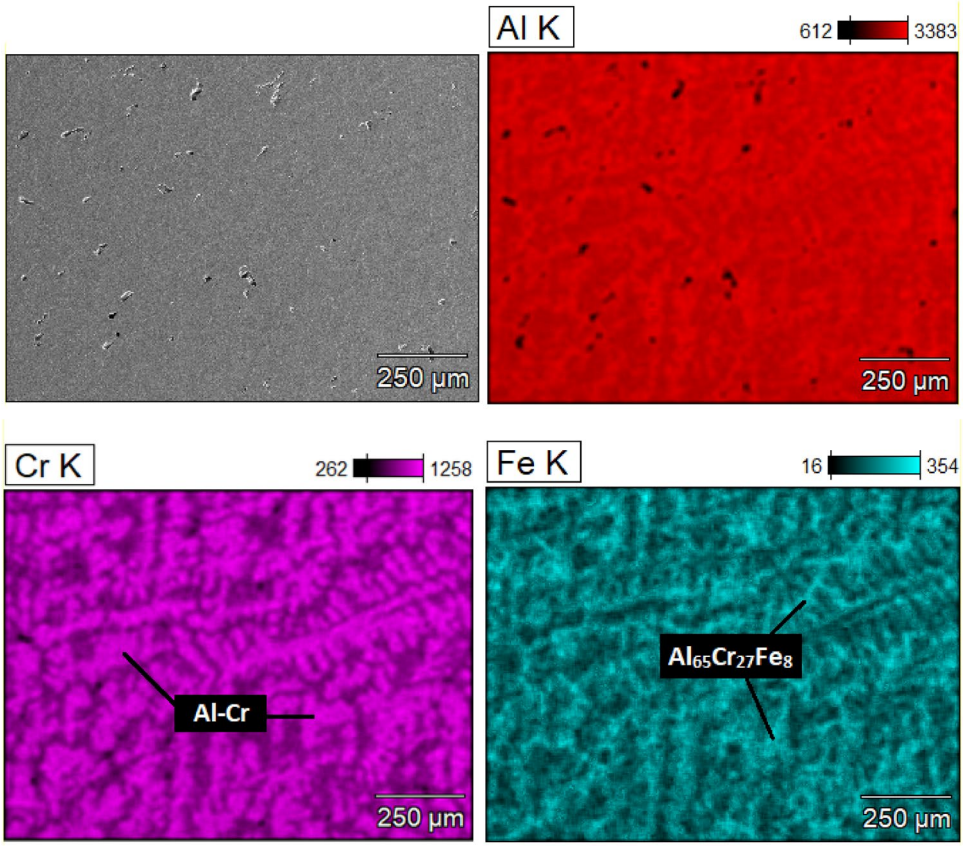

Figure 3. EDX maps of $Al_{71}Cr_{24}Fe_5$ alloy in a form of ingot.

Al–Cr–Fe alloys were described in the literature primarily in terms of the formation of structurally complex phases. Ura-Binczyk et al.[4,11] studied a polycrystalline alloy of $Al_{64.2}Cr_{27.2}Fe_{8.1}$, which was produced by hot press sintering of the intermetallic powders and heat treated. The authors[11] pointed out that γ-Al_8Cr_5 phase identified by XRD is isostructural with $Al_{65}Cr_{27}Fe_5$. In this study, the $Al_{65}Cr_{27}Fe_6$ phase had lattice parameters a = b = 12.6963 and c = 7.9211 and the angles between them α = β = 90° and γ = 120° in the hexagonal notation, which is consistent with the data reported in the articles[11,16]. According to report presented by Veys et al.[19] the phase of $Al_{65}Cr_{27}Fe_8$ has γ-brass structure and is isostructural to cubic Al_9Cr_4 (with lattice parameters a = 9.4 Å).

In this work, for the multiphase $Al_{71}Cr_{24}Fe_5$ alloy, the Al_8Cr_5 phase was also identified for both cooling rates. The lattice parameters of which a = b = c = 7.8050 and α = β = γ = 109.127° correspond to the α-Al_8Cr_5 phase, which corresponds to the rhombohedral system. The parameters of the unitary lattice cell are consistent with the description[12]. According to[10,12,21], the Al_8Cr_5 phase with a rhombohedral structure has a γ-brass structure.

Additionally, the results were compared with a study in which Al–Cr–Fe based alloys were cast[13]. Two phases were marked in the SEM image for the $Al_{66}Fe_{22}Cr_{12}$ alloy: α-Al_8Cr_5 and Al_5Fe_2. The microstructure is similar to that shown in Fig. 2 for $Al_{65}Cr_{20}Fe_{15}$[13].

Many researchers study the surface properties of complex metallic alloys because of the specific electronic structure associated with high symmetry clusters and unit cells made of thousands of atoms. Quasicrystals, which are included in the group of complex metallic alloys, are characterized by a low coefficient of friction and high wear resistance[2]. To describe abrasion resistance, tribological tests using the pin-on-disc method were performed. The test measurements with the parameters described in article[22] were carried out, however, no clearly signs of wear were observed, due to the low linear speed 0.05 m/s and the distance 8 m as well as relatively low load (F_N = 2 N). We used the parameters described in[23]. Figure 6 presents a graph of the dependence of the friction coefficient on the distance, which was recorded during the pin-on-disc for $Al_{65}Cr_{20}Fe_{15}$ and $Al_{71}Cr_{24}Fe_5$ in the form of ingots. It could be observed that the friction coefficient decreased to values of approximately 0.46 ($Al_{65}Cr_{20}Fe_{15}$) and 0.5 ($Al_{71}Cr_{24}Fe_5$) in the initial stage of the study. The gradual increase was visible after a distance of 25 m, stabilization occurred, in which the mean value of the coefficient of friction was 0.6 for $Al_{71}Cr_{24}Fe_5$ and 0.55 for $Al_{65}Cr_{20}Fe_{15}$. Based on the measurements conducted, it is visible that the $Al_{65}Cr_{20}Fe_{15}$ binary phase alloy was characterized by a lower friction coefficient compared to the $Al_{71}Cr_{24}Fe_5$ multiphase alloy.

The results of pin-on-disc tests were also described in[24], which compared the Al–Cu–Fe–Cr and Al–Cu–Fe alloys used for the coatings. It could be compared that for the chemical composition with the addition of chromium, the friction coefficient was similar to the results described in this article for $Al_{65}Cr_{20}Fe_{15}$ and $Al_{71}Cr_{24}Fe_5$ alloys (μ ≈ 0.6)[24]. Dubois et al.[25,26] compared the results of tribological tests for CMA alloys with different chemical compositions. In the publication, the orthorhombic Al–Cr–Fe and γ-Al–Cr–Fe alloys show the values of the

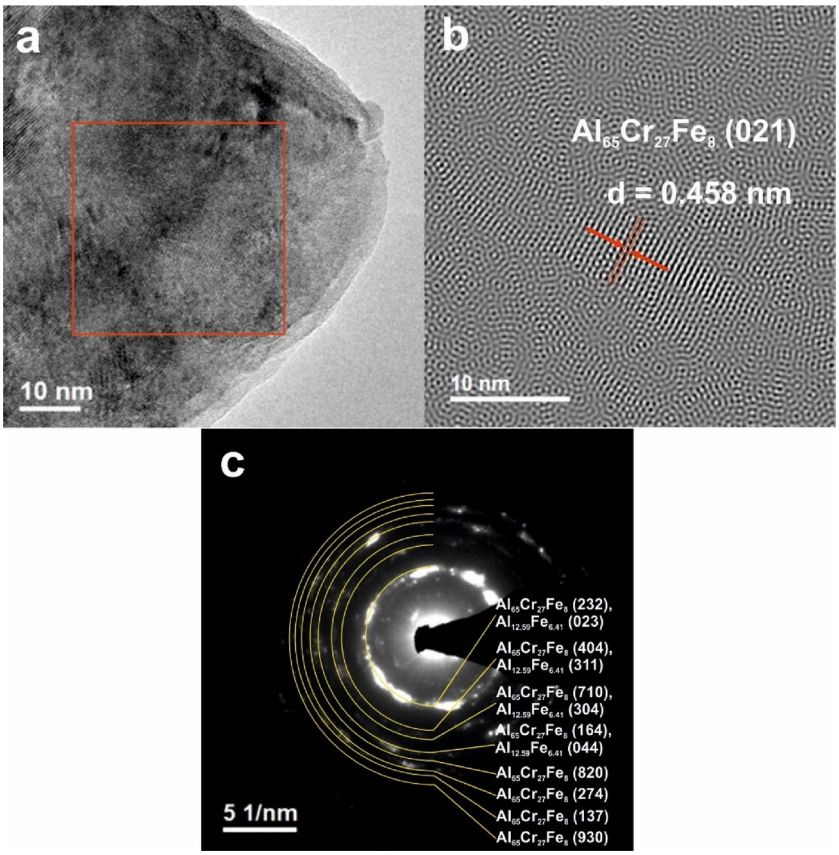

Figure 4. HRTEM image (**a**), IFT image (**b**) and SAED patterns (**c**) of $Al_{65}Cr_{20}Fe_{15}$ plate.

friction coefficient in the range of 0.5 ÷ 0.6. However, it should be noted that in publications[25,26] the pin-on-disc studies were carried out under vacuum. The authors[25,26] noted that the characteristic friction values are lower than in the air atmosphere. This is because the oxide layer has a significant influence on the measured value of the friction coefficient. Taking into account the fact that the alloys described in our work are binary and multiphase, it could be assumed that the wear resistance is similar to the single phase alloys[25,26].

Figure 7 shows the morphology of the wear tracks studied by SEM. It could be observed that three types of wear mechanisms dominated the trace of formation: plastic deformation, delamination, and oxidation. The identification of wear mechanisms was supported by the results described in paper[27]. Duckham et al.[28] investigated the wear resistance of quasicrystalline Al–Pd–Mn and Al–Ni–Co alloys. Wear tracks were also observed after pin-on-disc tests using microscopic methods. The authors[28] paid attention to the characteristic cracks that also appeared for the $Al_{65}Cr_{20}Fe_{15}$ and $Al_{71}Cr_{24}Fe_5$ alloys studied. This mechanism is called by[28] as the ring cracks, characteristic of brittle materials, which indicates the maximum tensile stress. The article[28] also describes the partial removal of the material, which is a delamination. The publications of Dubois et al.[25,26] described the phenomenon of oxidation during pin-on-disc tests caused by the air atmosphere, which was observed using SEM in the form of oxide debris. Furthermore, wear track width measurements were carried out, the mean values of which were 1.23 (± 0.05) and 1.27 (± 0.07) for the $Al_{65}Cr_{20}Fe_{15}$ and $Al_{71}Cr_{24}Fe_5$ alloy, respectively. However, the literature lacks data on the width of the wear tracks for similar alloys and the same experimental conditions.

The results of the average hardness measurements by the Vickers method together with the standard deviation for the $Al_{65}Cr_{20}Fe_{15}$ and $Al_{71}Cr_{24}Fe_5$ alloys in the form of ingots and plates are presented in the form of a bar graph in Fig. 8. $Al_{65}Cr_{20}Fe_{15}$ in the form of ingots with a binary phase structure showed an average value of 917 (± 30) $HV_{0.1}$, while the multiphase $Al_{71}Cr_{24}Fe_5$ 728 (± 34) $HV_{0.1}$. In the case of both chemical compositions, a clear effect of the application of the increased cooling rate of the liquid state was observed due to the values obtained of 943 (± 20) $HV_{0.1}$ for $Al_{65}Cr_{20}Fe_{15}$ and 802 (± 43) $HV_{0.1}$ for $Al_{71}Cr_{24}Fe_5$. The values obtained seem to be interesting due to the data in the comparison of the literature[25,26] according to which the hardness for γ-Al–Cr–Fe is just over 700 HV. Another article[2] presents the mean value of Vickers hardness for γ-$Al_{67.6}Cr_{23.3}Fe_{9.1}$ 840 (± 50) HV.

According to Dubois[29], quasicrystals and their approximants with good lattice excellence are characterized by diamagnetic properties in a wide range from ~ 50 K to the melting point. Among others, quasicrystalline Al-Cu-Fe alloys at the temperature of 2–300 K (− 271–27 ℃) showed diamagnetic properties[30]. According to the article[30], the paramagnetic properties for Al–Cu–Fe alloys result from the participation of crystalline phases or structural defects. The $Al_{86}Cr_8Fe_6$[31], $Al_{61.3}Cr_{31.1}Fe_{7.6}$[32], $Al_{80}Cr_{15}Fe_5$[33] alloys were characterized by paramagnetic properties. According to Bihar et al.[32], in the γ-AlCrFe approximant, the iron atoms are carriers of the magnetic moments. Therefore, as a result of the presence of two and many phases in the structure of the examined alloys,

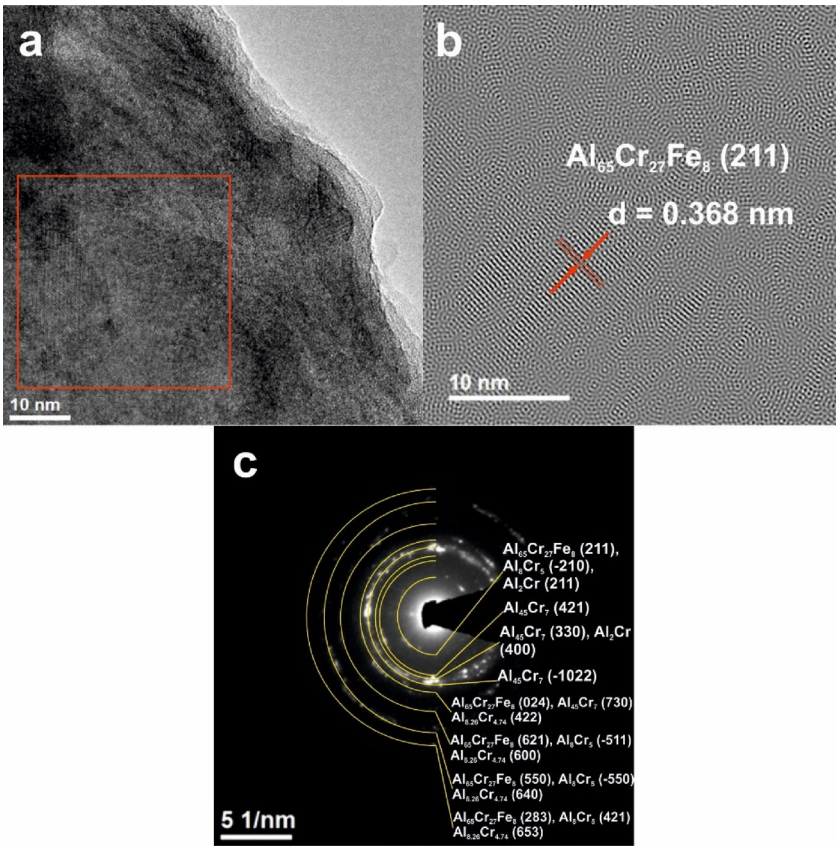

Figure 5. HRTEM image (**a**), IFT image (**b**) and SAED patterns (**c**) of $Al_{71}Cr_{24}Fe_5$ plate.

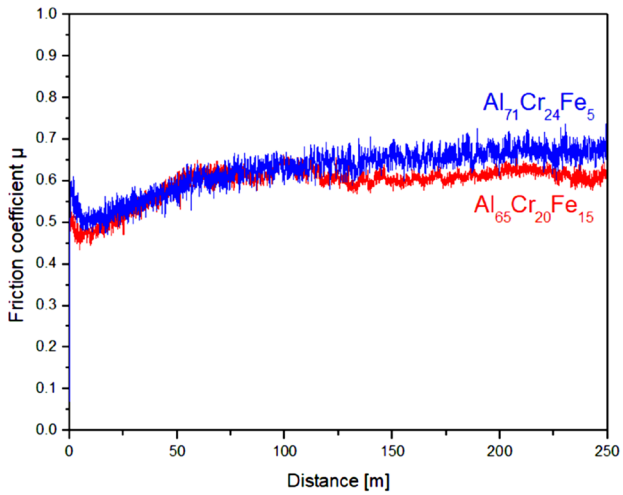

Figure 6. Pin-on-disc curves of $Al_{65}Cr_{20}Fe_{15}$ and $Al_{71}Cr_{24}Fe_5$ (ingots) as the relation of friction coefficient in the function of sliding distance.

magnetic tests seem to be a significant supplement to the current state of knowledge. Especially since there still exists a small amount of data on the magnetic properties of structurally complex alloys. Changes in magnetization in a function of magnetic field for $Al_{65}Cr_{20}Fe_{15}$ and $Al_{71}Cr_{24}Fe_5$ in the form of ingots and plates were illustrated in Fig. 9. The values of saturation magnetization (M_s) and coercivity (H_c) were listed in Table 1. In numerous studies, the influence of the structure on the magnetic properties was observed. In the case of the $Al_{65}Cr_{20}Fe_{15}$ alloy, the saturation magnetization was higher for the ingot form. The relationship was opposite and a lower value was noted for the ingot of the $Al_{71}Cr_{24}Fe_5$ composition. The coercivity was several times higher for the plates in

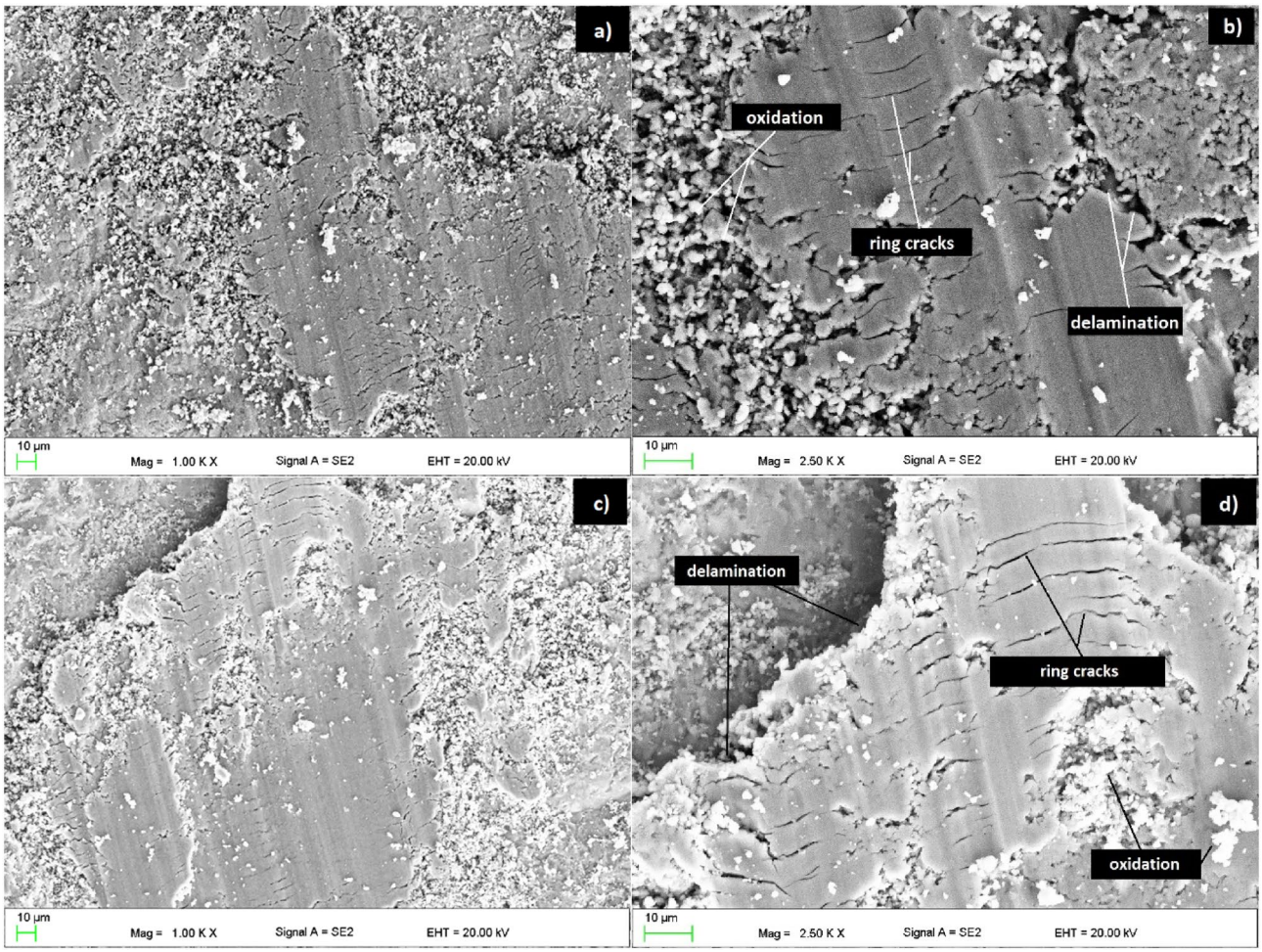

Figure 7. Surface morphology of the pin-on-disc friction track of (**a**, **b**) $Al_{65}Cr_{20}Fe_{15}$, (**c**, **d**) $Al_{71}Cr_{24}Fe_5$ alloys in a form of ingots.

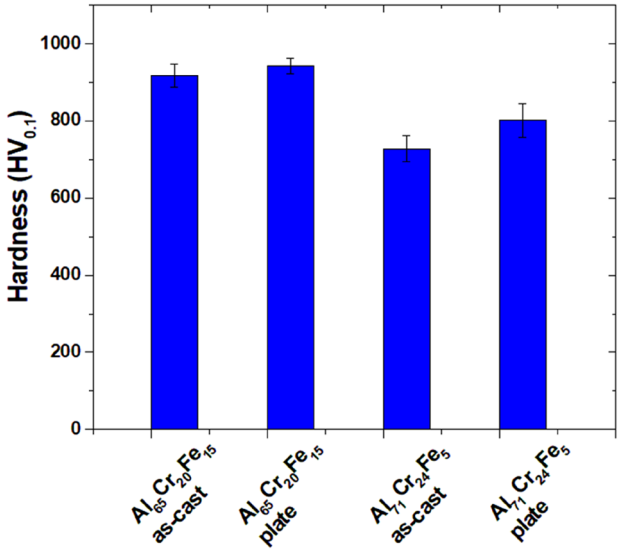

Figure 8. Comparison of hardness for $Al_{65}Cr_{20}Fe_{15}$ and $Al_{71}Cr_{24}Fe_5$ alloys in a form of ingots and plates.

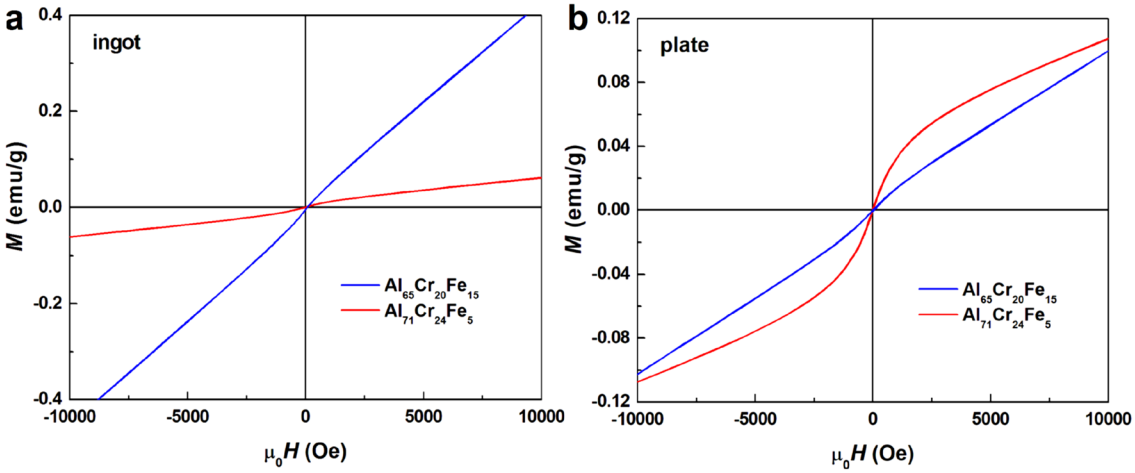

Figure 9. Magnetization (M) as a function of the magnetic field (μ_0H) at room temperature for $Al_{65}Cr_{20}Fe_{15}$ and $Al_{71}Cr_{24}Fe_5$ alloys in a form of ingots (**a**) and plates (**b**).

Sample	Type	M_s (emu/g)	H_c (Oe)
$Al_{65}Cr_{20}Fe_{15}$	Ingot	0.43	3.93
	Plate	0.09	27.69
$Al_{71}Cr_{24}Fe_5$	Ingot	0.06	5.23
	Plate	0.11	21.85

Table 1. The magnetic properties of $Al_{65}Cr_{20}Fe_{15}$ and $Al_{71}Cr_{24}Fe_5$ determined by analysis of the magnetization changes as a function of magnetic field (M_s, saturation magnetization; H_c, coercivity).

both chemical compositions. It may be related to changes in the structure under the influence of the cooling rate from the liquid state. In work[34] for Fe-based alloys with nanocrystalline structure, changes in coercivity resulting from grain growth after annealing were observed. In this work, the opposite phenomenon was observed because increasing casting conditions lead to fragmentation of the structure. The alloys studied showed paramagnetic properties. On the basis of the obtained results, a decrease of magnetic properties is visible along with an increase in the cooling rate from the liquid state for the $Al_{65}Cr_{20}Fe_{15}$ alloy and an increase for the $Al_{71}Cr_{24}Fe_5$ alloy. Paramagnetic properties were also described in[2,33] for the single phase $Al_{80}Cr_{15}Fe_5$ SCAP-type alloy. Furthermore, polycrystalline, structurally complex $Al_{86}Cr_6Fe_6$[31] and $Al_{61.3}Cr_{31.1}Fe_{7.6}$[32] alloys were previously described in the literature as paramagnets. Based on the research conducted, it could be concluded that the presence of crystalline phases in the $Al_{65}Cr_{20}Fe_{15}$ and $Al_{71}Cr_{24}Fe_5$ alloys did not change the magnetic properties at room temperature.

The corrosion resistance of Al–Cr–Fe alloys was reported in the paper[20]. Electrochemical measurements of the open circuit potential as a function of time and potentiodynamic polarization curves were recorded in a 3.5% NaCl aqueous solution at a temperature of 25 °C. Electrochemical impedance spectroscopy tests were also carried out. The electrochemical parameters, such as E_{OCP}, E_{corr}, R_p, and j_{corr} for studied Al-Cr-Fe alloys varied, which indicates differences in the corrosion mechanism. Among others, the $Al_{65}Cr_{20}Fe_5$ alloy in the form of plate showed a corrosion potential closer to the positive values, although a higher polarization resistance was observed for the $Al_{71}Cr_{24}Fe_5$ plate. Analysis of corrosion products is a useful tool to assess the corrosion behavior of materials; therefore, this article presents the results of the XPS analysis for $Al_{65}Cr_{20}Fe_{15}$ and $Al_{71}Cr_{24}Fe_5$ alloys in the form of plates after corrosion tests[35].

The XPS survey spectra for the surface of $Al_{65}Cr_{20}Fe_{15}$ (a) and $Al_{71}Cr_{24}Fe_5$ (b) in the form of plates are presented in Fig. 10. The characteristic peaks (O1*s*, C1*s*, Al2*s*, Al2*p*, Cr2*p*, Cr3*p*) and the Auger spectrum (for O KLL and C KLL) were identified. High intensities relative to the binding energy of oxygen may indicate the formation of a passive layer in the tested plates. Figures 11 and 12 present the XPS core level lines of Al2*p*, Cr2*p*, Fe2*p*, O1s acquired during depth profile measurements for $Al_{65}Cr_{20}Fe_{15}$ and $Al_{71}Cr_{24}Fe_5$ plates, respectively. As one may notice at the surface, high binding energy Al2*p* and Cr2*p* peaks typical for oxides are evident. These results indicate the formation of a passive layer of Al_2O_3 and Cr_2O_3. Along with removing successive atomic layers by the argon beam, Al2*p* and Cr2*p* are typical for pure aluminium and chromium elements. It is worth noting that for both plate samples, the Fe2*p* line is typical for metallic iron with a spin–orbit splitting of about $\Delta E \approx 12.8$ eV. The XPS depth profiles for plates $Al_{65}Cr_{20}Fe_{15}$ (a) and $Al_{71}Cr_{24}Fe_5$ (b) are shown in Fig. 13. As the sputtering time and depth increased, the samples analyzed showed a significantly lower percentage atomic concentration of C1*s*, indicating the presence of carbon impurity usually accumulated on the surface. In the case of O1*s*, the same tendency can be noticed. Oxygen in the initial stage of sputtering may indicate the presence of oxygen, as a typical impurity on the surface that overlaps with oxygen formed by the passive layers. As successive atomic

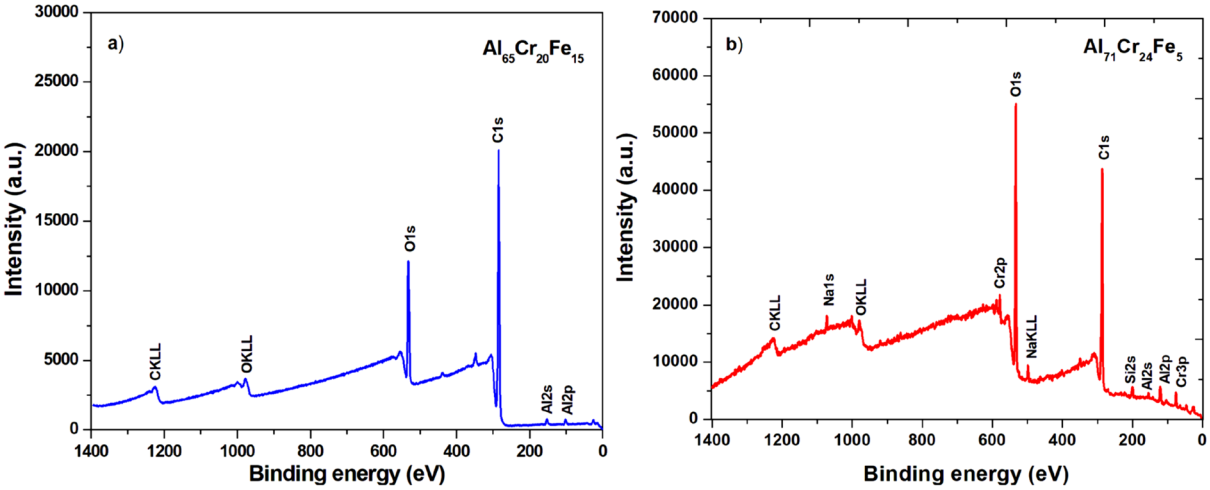

Figure 10. XPS survey spectra of $Al_{65}Cr_{20}Fe_{15}$ (**a**) and $Al_{71}Cr_{24}Fe_5$ (**b**) alloys in a form of plates after corrosion tests in 3.5% NaCl solution at 25 °C.

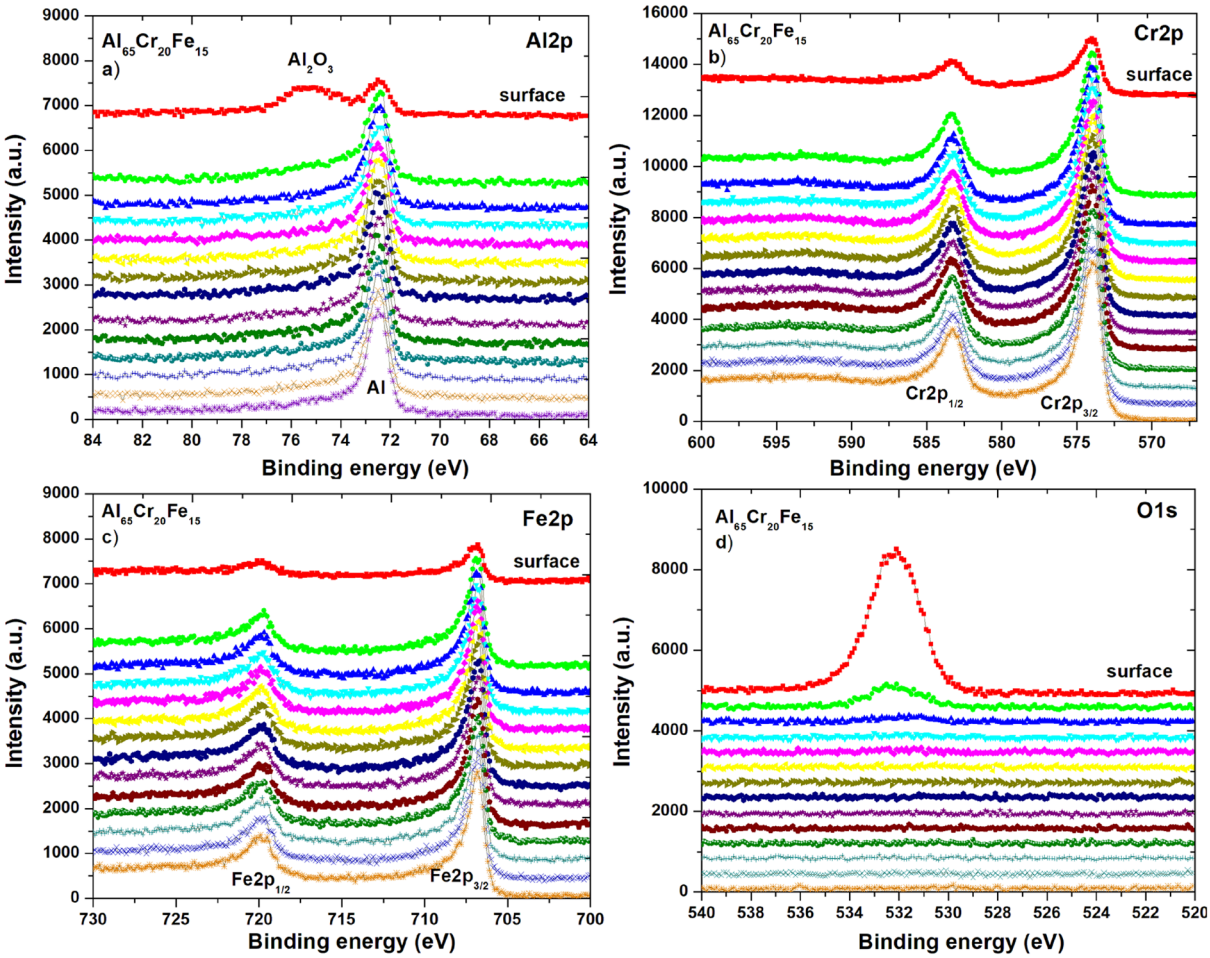

Figure 11. XPS core level lines of Al2*p* (**a**), Cr2*p* (**b**), Fe2*p* (**c**), O1*s* (**d**) of $Al_{65}Cr_{20}Fe_{15}$ plate after corrosion tests in 3.5% NaCl solution at 25 °C.

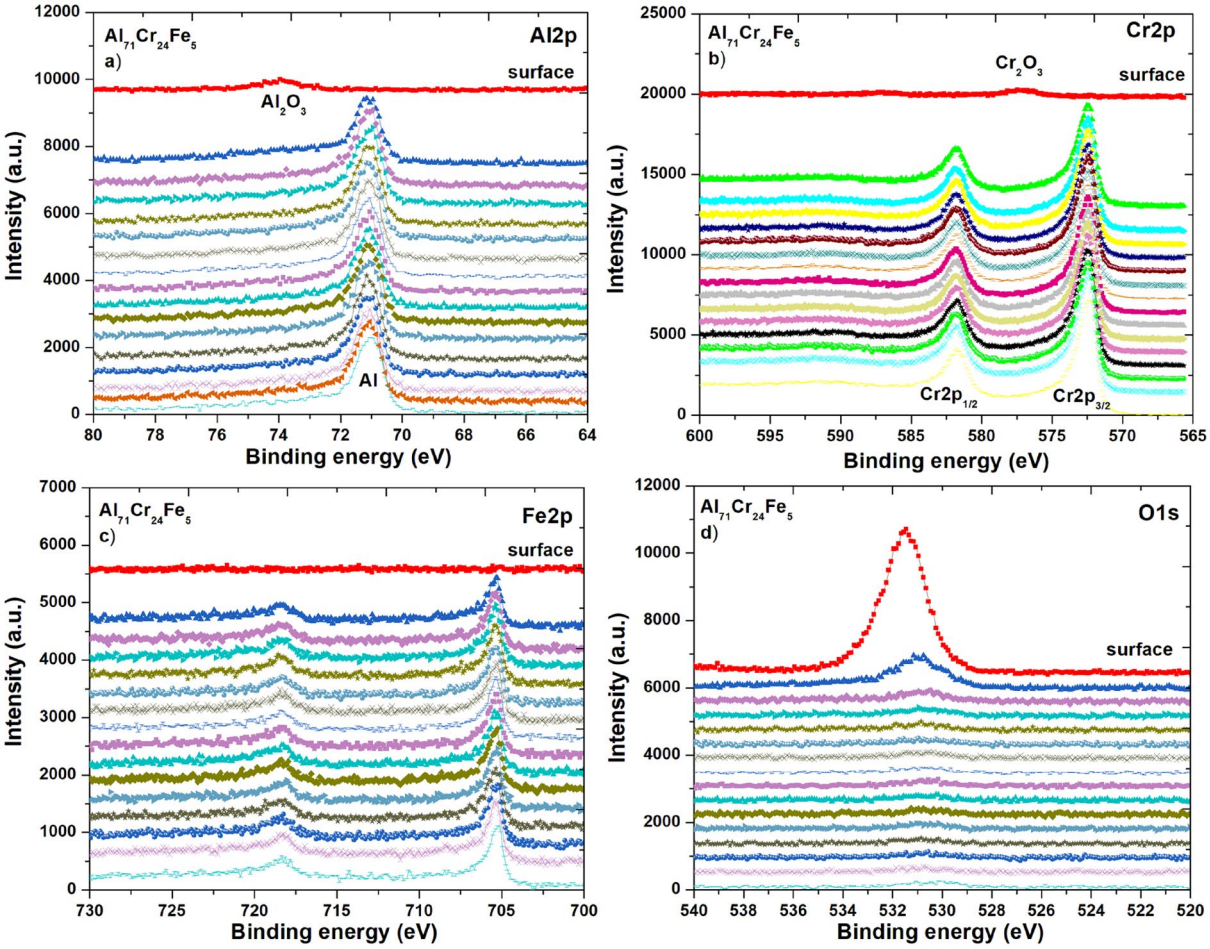

Figure 12. XPS core level lines of Al2*p* (**a**), Cr2*p* (**b**), Fe2*p* (**c**), O1*s* (**d**) of $Al_{71}Cr_{24}Fe_5$ plate after corrosion tests in 3.5% NaCl solution at 25 °C.

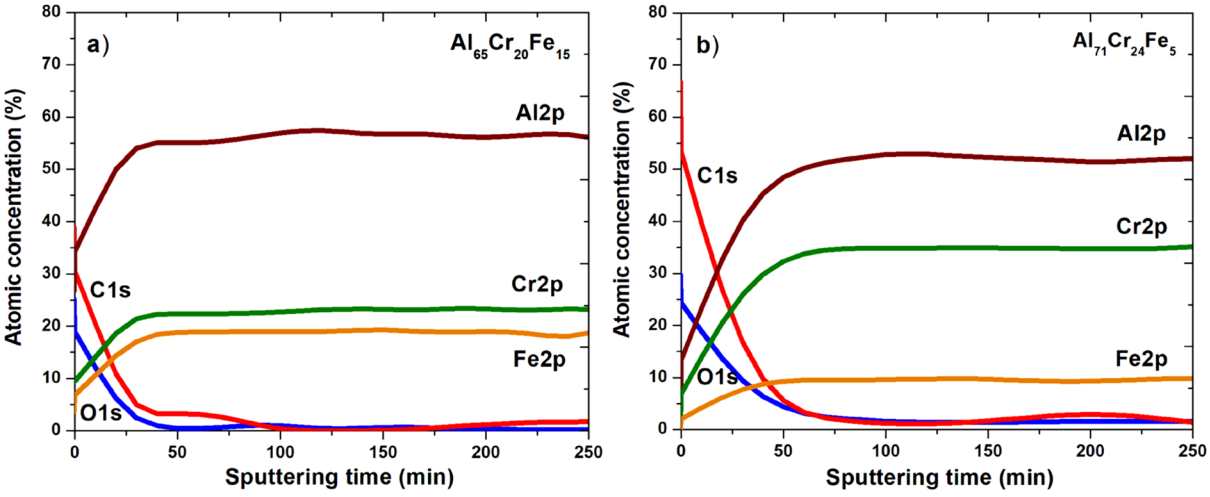

Figure 13. DP-XPS results for $Al_{65}Cr_{20}Fe_{15}$ (**a**) and $Al_{71}Cr_{24}Fe_5$ (**b**) alloys in a form of plates after corrosion tests in 3.5% NaCl solution at 25 °C.

layers of the argon beam are removed and the depth of the tested material increases, the atomic concentrations of Al, Cr, and Fe are higher than at the surface.

According to data from the work[1], the Al–Cr–Fe alloys should be characterized by good corrosion resistance, especially with high proportions of Al and Cr. These elements are passivating and allow the formation of a protective layer against further corrosion. Furthermore, Ott et al.[36] studied the polycrystalline γ-$Al_{64.2}Cr_{27.2}Fe_{8.1}$

alloy. Based on results[36], it was found that the addition of chromium is necessary for the stabilization of the passive layer. Therefore, the Cr_2O_3 was identified for the $Al_{71}Cr_{24}Fe_5$ alloy with a higher chromium content, which positively influences the corrosion resistance.

Conclusions

- Structural studies using ND, SEM–EDX, and TEM methods confirmed the presence of two phases for the $Al_{65}Cr_{20}Fe_{15}$ alloy and multiple phases for $Al_{71}Cr_{24}Fe_5$. Both alloys were characterized by the presence of the structurally complex alloy phase—$Al_{65}Cr_{27}Fe_8$. The Al_8Cr_5 phase with γ-brass structure was identified for $Al_{71}Cr_{24}Fe_5$ alloy in a form of ingot and plate.
- The binary phase $Al_{65}Cr_{20}Fe_{15}$ alloy showed a lower friction coefficient compared to the multiphase $Al_{71}Cr_{24}Fe_5$. The values of the coefficient of friction were similar for the single-phase CMA alloys described in the literature when the air atmosphere during the pin-on-disc tests was altered.
- The beneficial effect of the applied cooling rate on hardness was demonstrated for both chemical compositions. The binary phase $Al_{65}Cr_{20}Fe_5$ alloy was characterized by higher hardness values compared to the multiphase $Al_{71}Cr_{24}Fe_5$ alloy and the single phase Al–Cr–Fe alloy described in the literature.
- The $Al_{65}Cr_{20}Fe_{15}$ and $Al_{71}Cr_{24}Fe_5$ alloys studied showed paramagnetic properties. The $Al_{71}Cr_{24}Fe_5$ alloy with an increase in the cooling rate of the liquid state showed an increase of the magnetic values.
- The studied $Al_{65}Cr_{20}Fe_{15}$ and $Al_{71}Cr_{24}Fe_5$ alloys were characterized by the presence of passive oxide layers after electrochemical tests: $Al_{65}Cr_{20}Fe_{15}$ (Al_2O_3) and $Al_{71}Cr_{24}Fe_5$ ($Al_2O_3 + Cr_2O_3$). The higher intensity of oxides on the surface of $Al_{71}Cr_{24}Fe_5$ alloy was recorded because of higher chromium content that stabilizes a passive layer.

Data availability

The data and material generated during and/or analyzed during the current study are available from the corresponding author on reasonable request.

Received: 29 May 2022; Accepted: 2 August 2022
Published online: 20 August 2022

References

1. Ďuriška, L., Černičková, I., Priputen, P. & Palcut, M. Aqueous corrosion of aluminum-transition metal alloys composed of structurally complex phases: a review. *Materials (Basel).* **14**, 1–28 (2021).
2. Dubois, J. M. & Belin-Ferré, E. *Complex Metallic Alloys: Fundamentals and Applications* (WILEY-VCH Verlag GmbH & Co, 2010).
3. Dubois, J. M. An introduction to complex metallic alloys and to the CMA network of excellence. In *Basics of Thermodynamics and Phase Transitions in Complex Intermetallics* (ed. Belin-Ferré, E.) 1–29 (World Scientific, 2008).
4. Ura-Binczyk, E., Beni, A., Lewandowska, M. & Schmutz, P. Passive oxide film characterisation on Al–Cr–Fe and Al–Cu–Fe–Cr complex metallic alloys in neutral to alkaline electrolytes by photo- and electrochemical methods. *Electrochim. Acta* **139**, 289–301 (2014).
5. Dubois, J. M. Properties- and applications of quasicrystals and complex metallic alloys. *Chem. Soc. Rev.* **41**, 6760–6777 (2012).
6. Ovchinnikov, A., Smetana, V. & Mudring, A. V. Metallic alloys at the edge of complexity: Structural aspects, chemical bonding and physical properties. *J. Phys. Condens. Matter* **32**, 1–26 (2020).
7. Mayou, D. & Trambly de Laissardière, G. Quantum transport in quasicrystals and complex metallic alloys. In *Handbook of Metal Physics* (eds. Fujiwara, T. & Ishii, Y.) Vol. 3 209–265 (Elsevier Science, 2007).
8. Beni, A. *et al.* Passivation and localised corrosion susceptibility of new Al–Cr–Fe complex metallic alloys in acidic NaCl electrolytes. *Electrochim. Acta* **56**, 10524–10532 (2011).
9. Dong, C. The δ-Al_4Cu_9 phase as an approximant of quasicrystals. *Philos. Mag. A* **73**, 1519–1528 (1995).
10. Geng, X., Wen, B. & Fan, C. Crystal structure of the Al_8Cr_5 -type intermetallic $Al_{7.85}Cr_{5.16}$. *IUCrData* **5**, x200422 (2020).
11. Ura-Binczyk, E. *et al.* Passivation of Al–Cr–Fe and Al–Cu–Fe–Cr complex metallic alloys in 1M H_2SO_4 and 1M NaOH solutions. *Corros. Sci.* **53**, 1825–1837 (2011).
12. Demange, V., Ghanbaja, J., Machizaud, F. & Dubois, J. M. About γ-brass phases in the Al–Cr–Fe system and their relationships to quasicrystals and approximants. *Philos. Mag.* **85**, 1261–1272 (2005).
13. Rank, M., Franke, P., Hoffmann, J. & Seifert, H. J. Experimental investigation of phase equilibria in the Al–Cr–Fe system. *Calphad* **66**, 1–12 (2019).
14. Butler, T. M. & Weaver, M. L. Oxidation behavior of arc melted AlCoCrFeNi multi-component high-entropy alloys. *J. Alloys Compd.* **674**, 229–244 (2016).
15. Massalski, T. B. The Al–Cu (Aluminum–Copper) system. *Bull. Alloy Phase Diagrams* **1**, 27–33 (1980).
16. Grushko, B., Kowalska-Strzęciwilk, E., Przepiórzyński, B. & Surowiec, M. Investigation of the Al–Cr γ-range. *J. Alloys Compd.* **402**, 98–104 (2005).
17. Grushko, B. *et al.* Complex intermetallics in Al–Cu–Cr system. *J. Alloys Compd.* **442**, 114–116 (2007).
18. Grushko, B., Kowalska-Strzęciwilk, E., Przepiórzyński, B. & Surowiec, M. An investigation of the Al–Cu–Cr phase diagram: Phase equilibria at 800–1000 °C. *J. Alloys Compd.* **417**, 121–126 (2006).
19. Veys, D. *et al.* Chemical surface ageing in ambient conditions of an Al–Fe–Cr approximant phase. *J. Phys. Condens. Matter* **19**, 1–15 (2007).
20. Młynarek-Żak, K. *et al.* Electrochemical characterization of rapidly solidified Al-(Cr, Cu, Ni, Y, Zr)-Fe alloys. *Electrochim. Acta* **409**, 1–17 (2022).
21. Khoruzha, V. G., Kornienko, K. E., Pavlyuchkov, D. V., Grushko, B. & Velikanova, T. Y. The Al–Cr–Fe phase diagram: I—Phase equilibria at subsolidus temperatures over composition range 58–100 at.% Al. *Powder Metall. Met. Ceram.* **50**, 83–97 (2011).
22. Cavalcante Guedes de Lima, D. *et al.* Indirect assessment of the surface energy of the Al–Cu–Fe quasicrystal. *J. Mater. Sci.* **51**, 4070–4078 (2016).
23. Sordelet, D. J., Kim, J. S. & Besser, M. F. Dry sliding of polygrained quasicrystalline Al–Cu–Fe alloys. *Mater. Res. Soc. Symp. Proc.* **553**, 459–470 (1999).

24. Wolf, W. *et al.* Wear and corrosion performance of Al–Cu–Fe–(Cr) quasicrystalline coatings produced by HVOF. *J. Therm. Spray Technol.* **29**, 1195–1207 (2020).
25. Dubois, J. M. & Belin-Ferré, E. Friction and solid-solid adhesion on complex metallic alloys. *Sci. Technol. Adv. Mater.* **15**, 1–20 (2014).
26. Dubois, J. M., Brunet, P., Costin, W. & Merstallinger, A. Friction and fretting on quasicrystals under vacuum. *J. Non. Cryst. Solids* **334–335**, 475–480 (2004).
27. Li, N. & Yan, H. The effects of rare earth pr and heat treatment on the wear properties of AZ91 alloy. *Curr. Comput. Aided Drug Des.* **8**, 1–13 (2018).
28. Duckham, A., Shechtman, D. & Grushko, B. Influence of grain orientation on friction and wear behavior in quasicrystalline alloys. *Mater. Res. Soc. Symp. Proc.* **643**, 811–816 (2001).
29. Dubois, J. M. *Useful Quasicrystals*. (World Scientific, 2003).
30. Klein, T., Berger, C., Mayou, D. & Cyrot-Lackmann, F. Proximity of a metal-insulator transition in icosahedral phases of high structural quality. *Phys. Rev. Lett.* **66**, 2907–2910 (1991).
31. Stadnik, Z. M. & Müller, F. Thermal, structural and magnetic properties of icosahedral $Al_{86}Cr_8Fe_6$ alloy. *Philos. Magn. B* **71**, 221–238 (1995).
32. Bihar, Ž *et al.* Magnetic, electrical and thermal transport properties of Al–Cr–Fe approximant phases. *J. Alloys Compd.* **407**, 65–73 (2006).
33. Dolinšek, J. *et al.* Anisotropic electrical, magnetic and thermal transport properties of the $Al_{80}Cr_{15}Fe_5$ decagonal approximant. *Philos. Magn.* **88**, 2145–2153 (2008).
34. Carrillo, A., Daza, J., Saurina, J., Escoda, L. & Suñol, J. J. Structural, thermal and magnetic analysis of $Fe_{75}Co_{10}Nb_6B_9$ and $Fe_{65}Co_{20}Nb_6B_9$ nanostructured alloys. *Materials (Basel).* **14**, 1–12 (2021).
35. Duchoslav, J., Arndt, M., Keppert, T., Luckeneder, G. & Stifter, D. XPS investigation on the surface chemistry of corrosion products on ZnMgAl-coated steel. *Anal. Bioanal. Chem.* **405**, 7133–7144 (2013).
36. Ott, N., Beni, A., Ulrich, A., Ludwig, C. & Schmutz, P. Flow microcapillary plasma mass spectrometry-based investigation of new Al–Cr–Fe complex metallic alloy passivation. *Talanta* **120**, 230–238 (2014).

Author contributions

K.M-Ż. and R.B. developed the methodology and assumptions of the experiments. W.P. conducted and interpreted pin-on-disc and scanning electron microscopy studies. R.B. conducted the structural analysis using transmission electron microscopy. D.Ł. carried out HRTEM observations. A.B. conducted and interpreted XPS studies. P.G. carried out VSM tests. I.D. and A.S. conducted research and analysis with the use of neutron diffraction. K.M-Ż. conducted and interpreted Vickers hardness measurements. K.M-Ż. wrote the main manuscript text. R.B. was responsible for supervision over research works. All authors reviewed and approved the manuscript.

Funding

The work was supported by the National Science Centre of Poland under research project no. 2018/29/B/ST8/02264 and the statutory subsidy of the Faculty of Mechanical Engineering of the Silesian University of Technology no. 10/010/BKM22/1107.

Competing interests

The authors declare no competing interests.

Additional information

Correspondence and requests for materials should be addressed to K.M. or R.B.

Reprints and permissions information is available at www.nature.com/reprints.

Publisher's note Springer Nature remains neutral with regard to jurisdictional claims in published maps and institutional affiliations.